Carbohydrate Polymers 208 (2019) 382–390

Contents lists available at ScienceDirect

Carbohydrate Polymers

journal homepage: www.elsevier.com/locate/carbpol

Melt-processing of bionanocomposites based on ethylene-co-vinyl acetate and starch nanocrystals

Valentina Sessini[a,b], Jean-Marie Raquez[c,*], José Maria Kenny[a], Philippe Dubois[c], Laura Peponi[b,*]

[a] Dipartimento di Ingegneria Civile e Ambientale, Università di Perugia, Strada di Pentima, 05100 Terni, Italy
[b] Instituto de Ciencia y Tecnología de Polímeros, ICTP-CSIC, calle Juan de la Cierva 3, 28006, Madrid, Spain
[c] Laboratory of Polymeric and Composite Materials, University of Mons – UMONS, Place du Parc 23, B-7000 Mons, Belgium

ARTICLE INFO

Keywords:
Starch nanocrystals
Solvent-free process
Melt-processing
EVA
Hydrogen bonding

ABSTRACT

Starch nanocrystals (SNCs) were successfully synthesized by acid hydrolysis of waxy barley starch and were characterized by X-ray diffraction, scanning and transmission electron microscopy. Nanocomposites based on ethylene-co-vinyl acetate (EVA) and SNCs were produced by melt-processing using a microextruder. Interesting is to note that SNCs do not lose their crystalline nature during melt-processing. Moreover, the mechanical and thermal properties of the neat matrix were improved by the addition of SNCs thanks to the strong hydrogen bonding between the nanofillers surface and the acetate groups of the matrix. The introduction of 2 wt.% and 5 wt.% of SNCs into the matrix, lead to an increase of its elastic modulus of about 50% and 100%, respectively. Moreover, the addition of SNCs provoked an increase of the thermal stability of about 10 °C respect to the neat matrix. These results clearly revealed the possibility to introduce SNCs in a polymeric matrix by extrusion enabling to reach materials with enhanced mechanical and thermal properties due to beneficial hydrogen bonding between SNCs and EVA.

1. Introduction

In the last several years, polymeric nanocomposites based on bio-nanofillers have attracted both academic and industrial attentions due to the increasing interest on designing new “green” bionanocomposites based on renewable nanofillers (Darder, Aranda, & Ruiz-Hitzky, 2007; Hebeish, El-Rafie, El-Sheikh, & El-Naggar, 2014). In particular, nano-whiskers and nanocrystals obtained from natural polymers have been applied to reinforce biodegradable or non-biodegradable polymeric matrix. In general, these kind of natural nanofillers are produced by acid hydrolysis of natural polysaccharides, such as cellulose, chitin and starch and they are obtained as aqueous suspensions (Le Corre, Bras, & Dufresne, 2010; Lin, Huang, Chang, Anderson, & Yu, 2011; Navarro-Baena, Kenny, & Peponi, 2014). For this reason, most investigations have focused on the use of hydrosoluble (Chen, Cao, Chang, & Huneault, 2008) or at least hydrodispersible, or latex-form polymers (Rajisha, Maria, Pothan, Ahmad, & Thomas, 2014) as matrix in order to reach good fillers dispersion. In general, due to their polar character, to reach a good dispersion of polysaccharides nanocrystals into apolar polymeric matrices is a very interesting challenge (Peponi, Puglia, Torre, Valentini, & Kenny, 2014). Polysaccharide nanocrystals possess a reactive surface related with hydroxyl groups, providing the possibility of extensive chemical modifications that open interesting possibilities for nanocomposite processing (Goffin, Habibi, Raquez, & Dubois, 2012; Haaj, Thielemans, Magnin, & Boufi, 2014; Hebeish et al., 2014; Jiahui et al., 2008; Labet, Thielemans, & Dufresne, 2007; Sessini, Arrieta, Fernández-Torres, & Peponi, 2018; Sessini, Navarro-Baena et al., 2018).

Starch is certainly one of the most versatile biodegradable materials for potential use in polymer technology. Indeed, it can be converted into chemicals for the production of synthetic polymers, it can be used for the production of biopolymers through fermentative processes and it can be also hydrolyzed to be a monomer or oligomer. Finally, it can be used as polymeric materials and such as fillers for other polymers (Carvalho, 2013). Interestingly, starch nanocrystals (SNCs) have recently been used as nanofillers in polymeric matrices such as natural rubber (Rajisha et al., 2014), poly-vinyl alcohol (Chen et al., 2008), waterborne polyurethanes (Wang, Tian, & Zhang, 2010) and thermoplastic starch (Li et al., 2015; Sessini, Arrieta et al., 2018; Sessini, Navarro-Baena et al., 2018; Sessini, Arrieta, Kenny, & Peponi, 2016) showing increasing reinforcing effects as well as good barrier properties.

Very few studies have been reported concerning the processing of SNCs reinforced nanocomposites by solvent-free methods. Pereda et al. reported the design of nanocomposites based on polyethylene by

* Corresponding authors.
E-mail addresses: JeanMarie.RAQUEZ@umons.ac.be (J.-M. Raquez), lpeponi@ictp.csic.es (L. Peponi).

https://doi.org/10.1016/j.carbpol.2018.12.095
Received 3 September 2018; Received in revised form 28 December 2018; Accepted 30 December 2018
Available online 31 December 2018
0144-8617/

wrapping the SNCs with a polymer (polyethylene oxide) bearing moieties susceptible to interact physically with the nanoparticle surface and with the apolar matrix. Improved dispersaibility and reduced thermal degradation of the nanoparticles were observed showing the compatilizing effect of PEO (Pereda, Kissi, & Dufresne, 2014).

Copolymers of ethylene-co-vinyl acetate (EVA) are a class of widely used polymers, with a variety of industrial applications such as flexible packaging, membranes, footwear, biomedical applications, *etc.* (Peeterbroeck, Alexandre, Jérôme, & Dubois, 2005; Sonia & Dasan, 2013). Interestingly, EVA copolymers are widely used as wood and paper adhesives because of their good interaction with cellulose materials. Indeed EVA is composed of polar vinyl acetate (VA) groups randomly distributed in the apolar ethylene chains. The degree of polarity of EVA increases by increasing the VA content. Interaction between EVA and polar fillers is proportional to the polarity of EVA. In this context, in literature is reported that, the higher is the polarity of EVA, the stronger is the interaction between EVA and silicate as well as cellulose nanowhiskers, leading to a good dispersion of the nanofillers into the polymeric matrix and better reinforcing effect. (Chauve, Heux, Arouini, & Mazeau, 2005; Zhang & Sundararaj, 2004). However, the interactions between EVA and the nanofiller surface are limited by the conformational freedom of the polymer that control the number of acetate groups able to be engaged with hydroxyl groups at the nanofiller surface (Chauve et al., 2005).

Besides, in many cases EVA applications are limited due to its low tensile strength, thermal stability, and high flammability (Bidsorkhi, Adelnia, Pour, & Soheilmoghaddam, 2015; Gao, Beyer, & Yuan, 2005). To overcome these deficiencies, incorporating nanofillers into EVA represents an excellent way to get high-performance EVA-based nanocomposites. At this regard, several investigations have been reported in literature, including the incorporation of graphite oxide (Sengupta, Bhattacharya, Bandyopadhyay, & Bhowmick, 2011), sepiolite (Bidsorkhi, Soheilmoghaddam, Pour, Adelnia, & Mohamad, 2014), montmorillonite (Alakrach, Osman, Noriman, Betar, & Dahham, 2016; Zanetti, Camino, Thomann, & Mülhaupt, 2001), organoclay (Zhang & Sundararaj, 2004), carbon nanotube (Morlat-Therias et al., 2007) and so on.

Despite an extensive search, based on our knowledge, no detailed study on EVA-based nanocomposites reinforced with SNCs processed by solvent-free methods has been reported in literature. For its properties and especially for its polarity, EVA is a perfect candidate to ensure a good dispersion of polar fillers like SNCs providing an interesting platform for the construction of EVA/SNCs nanocomposites with improved properties.

In this work, the preparation of EVA/SNCs nanocomposites by extrusion has been reported and a comprehensive evaluation of SNCs content on mechanical and thermal properties of nanocomposites has been investigated. X-ray diffraction, atomic force microscopy and field emission scanning electron microscopy confirmed the presence of well dispersed SNCs into the EVA matrix. The study clearly revealed the possibility to introduce SNCs in a polymeric matrix by extrusion enabling to reach materials with enhanced mechanical and thermal properties due to beneficial hydrogen bonding between SNCs and EVA.

2. Materials and methods

2.1. Materials

Commercial EVA copolymer with 19 wt.% VA content was purchased from Exxon Mobil Chemical Company. Waxy barley starch (WBS) was supplied by Lyckeby Culinar AB (Sweden). Sulfuric acid (H_2SO_4) was purchased from Sigma-Aldrich.

2.2. Starch nanocrystals synthesis

SNCs were synthesized by acid hydrolysis. WBS granules were mixed with 175 mL of 3.16 M sulfuric acid solution. The suspension was kept under 100 rpm mechanical stirring at 40 °C, using a silicon oil bath for 5 days. The final suspensions were washed by successive centrifugations in distilled water (10,000 rpm for 10 min) until reaching neutral pH and redispersed using Ultra Turrax for 5 min to avoid aggregates. The obtained suspensions were filtered on a filter tissue (113 Whatman) and storage at 4 °C (LeCorre, Bras, & Dufresne, 2012). Finally, it was freeze-dried (LIOALFA 6, Telstar) to obtain SNCs powder.

2.3. EVA/SNCs nanocomposites processing

Two nanocomposites with different SNCs content, *i.e.* 2 and 5 wt.%, have been processed and their properties were compared with those of neat EVA. First of all, in order to avoid the SNCs destructuration or gelatinization during the processing, EVA pellets and SNCs powder were dried for 24 h under vacuum at 35 °C. EVA/SNCs nanocomposites were obtained by a microextruder equipped with twin conical corotating screws (MiniLab Haake Rheomex CTW5, Thermo Scientific) with a capacity of 7 cm^3. A screw rotation rate of 75 rpm, temperature of 120 °C, and residence time of 4 min were used. The processed nanocomposites were named EVA-2SNC and EVA-5SNC highlighting the SNCs amount into the EVA matrix. The extruded nanocomposites were successively thermo-compressed in a Dr. Collin 200 mm × 200 mm press at 120 °C and 50 bars in order to obtain films to carry out their characterization.

2.4. Characterization techniques

The thermal properties were investigated by Differential Scanning Calorimetry (DSC) analysis. The dynamic DSC measurements were performed in a Mettler Toledo DSC822e instrument, under nitrogen flow (30 ml/min). Samples of about 10 mg were sealed in aluminum pans. Thermal cycles were composed by the following "heat/cool/heat" procedure: heating at 10 °C min^{-1} from −80 °C to 150 °C, cooling at 10 °C min^{-1} to −80 °C and heating again at 10 °C min^{-1} to 150 °C. The first scan was done to erase prior thermal history of the samples. From second and third scans, the crystallization temperature (T_c), glass transition temperature (T_g), melting temperature (T_m) and the melting enthalpy (ΔH_m) were obtained. Glass transition temperatures were determined at the inflection point. The degree of crystallinity (X_c) of each sample was calculated, according with the equation below:

$$X_c(\%) = \frac{\Delta H_m}{\Delta H_M^{100}} \times 100 \quad (1)$$

where, ΔH_m ΔH_M^{100} is the specific melting enthalpy for a 100% crystalline PE (293 J/g) as considering that VA comonomer units are not able to participate in the crystalline lattice (Brogly, Nardin, & Schultz, 1997)

Dynamic Mechanical Thermal Analisys (DMTA) of the samples was carried out using a DMA Q800 from TA Instrument in film tension mode with an amplitude of 5 μm, a frequency of 1 Hz, a force track of 125%, and a heating rate of 2 °C·min^{-1}. Samples subjected to DMA were cut from compression-molded thin films into regular specimens of approximately 20 mm × 5 mm × 0.60 mm.

Thermogravimetric analysis (TGA) was carried out using a TA-TGA Q500 thermal analyzer. Neat EVA and EVA/SNCs nanocomposites were analyzed by dynamic mode using about 10 mg of sample from room temperature to 800 °C at 10 °C min^{-1} under nitrogen flow (60 mL min^{-1}). Temperatures at the maximum degradation rate (T_{max}) were calculated from the first derivative of the TGA curves (DTG).

Attenuated total reflectance-Fourier transform infrared spectroscopy (ATR-FTIR) measurements were carried out with a Spectrum One FTIR spectrometer (Perkin Elmer instruments). Spectra were obtained in transmission mode at room temperature in the 4000-650 cm^{-1} region with a resolution of 4 cm^{-1} and 32 scans.

X-ray Diffraction (XRD) measurements were performed using a

Bruker D8 Advance instrument with a Cu Kα source (0154 nm) and a detector Vantec1. The scanning range was 4°-40°, step-size and count time per step were 0.023851° and 0.2 s, respectively.

The morphology of native WBS granules and SNCs were studied by Scanning Electron Microscopy (SEM PHILIPS XL30 with a tungsten filament). WBS and SNCs samples were dispersed in distilled water and ultrasonicated for 10 min. Then, a small droplet of the dilute suspension was deposited on glass sample holder and dried at room temperature. All the samples were gold/palladium coated by an automatic sputter coated Polaron SC7640. Field Emission Scanning Electron Microscope (FE-SEM, Hitachi S8000) in transmission mode was used to observe SNCs morphology as well as their dispersion into the EVA matrix in the nanocomposites. SNCs were dispersed in distilled water and ultrasonicated for 10 min. Then, a small droplet of the dilute suspension was deposited on a copper grid and dried at room temperature. The nanocomposite films were cut into ultra-thin sections with a microtome for FE-SEM observation. SNCs morphology was observed also with Transmission electron microscope (TEM) using a Philips CM200 electron microscope, using an accelerator of 120 kV.

Atomic force microscopy (AFM) experiments were performed in tapping mode, TM-AFM, using a Multimode AFM (VEECO Instruments, Santa Barbara, CA) equipped with a Nanoscope Iva control system (software version 6.14r1). Silicon tapping probes (RTESP, Veeco) were used with a resonance frequency of ˜300 kHz and a scan rate of 1 Hz. Smooth fracture surfaces of both nanocomposite bulk were cut by ultramicrotome equipped with a diamond knife to be observed by AFM.

Mechanical properties were determined using an Instron Universal Testing Machine at a strain rate of 150 mm min^{-1} in order to avoid the strain hardening effect of EVA. Tensile test measurements were performed on 5 dog-bone specimens with a width of 2 mm, thickness of 0.60 mm and leaving an initial length between the clamps of 20 mm. From these experiments were obtained the Young Modulus, as the slope of the curve between 0% and 2% of deformation, the elongation at break and the maximum stress reached.

3. Results and discussion

SEM micrograph of native WBS granules suspension in water is reported in Fig. 1.a. WBS granules showed a lenticular-like shape with a diameter of around 15–20 μm and homogeneous size distribution, in agreement with the literature (Fredriksson, Silverio, Andersson, Eliasson, & Åman, 1998). In general, starches are categorized in three crystalline types called A, B and C (Wang, Bogracheva, & Hedley, 1998) depending on their X-ray diffraction pattern. The differences in the crystalline structure could render different nanocrystals morphology (LeCorre, Bras, & Dufresne, 2011). A-type structure is frequently distinguished by strong reflections at 2θ = 15.11°, 17.14°, 18.14° and 26.27°, with some additional reflections at 2θ = 9.98°, 11.19°, 22.93°, 23.68°, 30.30° and 33.08° (Lopez-Rubio, Flanagan, Gilbert, & Gidley, 2008; Mutungi, Passauer, Onyango, Jaros, & Rohm, 2012). X-ray patterns of WBS granules and the obtained SNCs (WBSNC), are shown in Fig. 1.b. Acid hydrolysis treatment effectively led to remove the amorphous domains of starch granules while leaving the crystalline part intact. Indeed, X-ray patterns of native WBS as well as of WBSNCs display all the characteristic peaks of the A-type structure (2θ = 9.9°, 11.2°, 15°, 17.1°, 17.9°, 19.8°, 22.9°, 26.4°, 30.3°) according with their morphology. In Fig. 1.c and 1.d, the SEM and TEM micrographs of SNCs are reported, respectively. SNCs tended to self-aggregate after lyophilization but they preserve the same shape and homogeneous size distribution. They present a length of 35–50 nm and a width of 15–25 nm, in good agreement with the literature (Yixiang et al., 2014).

It is well known that the reinforcement effect of nanofillers depends on such factors as its dispersion into the polymeric matrix (Wang et al., 2010) and their interfacial interaction with the polymeric matrix (Chauve et al., 2005; Peponi et al., 2014).

At this regard, in order to study their interfacial interaction, ATR-FTIR spectra of the EVA/SNCs nanocomposites, SNCs and neat EVA are shown in Fig. 2. The ATR-FTIR spectra of neat EVA and its nanocomposites show the typical bands of vinyl acetate at 1737, 1238 and 1020 cm^{-1} and those of ethylene at 2917, 2850, 1464, 1371 and 719 cm^{-1}. These bands are in good agreement with the literature values (Bidsorkhi et al., 2015; Khodkar & Ebrahimi, 2011).

The bands at 2917 cm^{-1} and 2850 cm^{-1} in the spectra of EVA samples have been attributed to the asymmetric and symmetric vibrations of aliphatic groups $(-CH_2-)_n$, respectively. The 1737 cm^{-1} band corresponds to carbonyl stretching vibrations of the acetate groups. Furthermore, the spectrum of SNCs shows the typical bands of starch. The O—H stretching mode of starch was observed in the region of 3000 and 3600 cm^{-1} and the C–H stretching modes in the 2800–3000 cm^{-1} region. The band observed at 1642 cm^{-1} was attributed to the O—H bending of absorbed water in the SNCs. The stretching vibration of C–O bond in C–O—H and C–O—C group in the anhydrous glucose ring appeared at 1150, 1075, and 1005 cm^{-1}. Meanwhile, the shoulder absorption at 1045 cm^{-1} was associated with the crystalline phase of SNCs as reported in literature (Gong et al., 2016). Finally, the characteristic band of C–O—C ring vibration of starch was observed at 769 cm^{-1} (Kizil, Irudayaraj, & Seetharaman, 2002). The addition of SNCs into the EVA matrix enhances the intensity of the band at 1150 cm^{-1} compared to neat EVA spectrum. Moreover, increasing the amount of SNCs, in the EVA/SNCs nanocomposites spectra, this band appears shifted at higher values from 1150 cm^{-1} to 1153 and 1155 cm^{-1} for EVA-2SNC and EVA-5SNC, respectively. Simultaneously the intensity of the O—H stretching band of SNCs observed in the region of 3000 and 3600 cm^{-1} was almost absent for both EVA-2SNC and EVA-5SNC. The changes observed in the spectra of EVA/SNCs nanocomposites suggested the possible presence of hydrogen bonding interactions between SNCs and EVA matrix. Similar results were previously reported for EVA/halloysite and poly(vinyl alcohol)/SNCs nanocomposites (Bidsorkhi et al., 2015; Chen et al., 2008).

The physical interaction between EVA and SNCs was reflected also in the dispersion of the fillers into the polymer matrix that was studied by FE-SEM in transmission mode. The FE-SEM images at different magnification are shown in Fig. 3.

The FE-SEM images showed quite good dispersion of the SNCs in both nanocomposites confirming that during the melt-processing, the SNCs were not destructurated by maintaining their structural dimensions. The homogeneous dispersion of the SNCs in the EVA matrix depends on the interaction between the SNCs and the polar group of EVA, resulting in a good adhesion on the interfaces of SNCs and EVA matrix as it was previously demonstrated for poly(vinyl alcohol)/SNCs nanocomposites obtained by solvent casting (Chen et al., 2008). To further verify the presence of crystalline SNCs into the polymeric matrix, XRD measurements were performed and reported in Fig. 4.

A thermal treatment has been done on SNCs in order to simulate the thermal processing conditions used to obtain the nanocomposites, submitting them at 120 °C for 3 min, naming them SNCs TT in Fig. 4.a. Then, the XRD of SNCs has been performed showing that the crystalline structure of SNCs was kept even after the thermal treatment.

As reported in Fig. 4.a, X-ray patterns of SNCs display all the characteristic peaks of the A-type structure (2θ = 9.9°, 11.4°, a strong intensity peak at 15.1°, a double peak at 17.1° and 17.9° and a last strong intensity peak at 23.1°) with a broad peak at around 2θ = 30.3°. The thermal treatment did not change the crystalline structure of the SNCs.

Fig. 4.b indicates XRD patterns of neat EVA and its nanocomposites. Neat EVA showed an X-ray pattern with strong and broad crystalline peak at 2θ = 21.5°, resulting mainly from the crystalline region of EVA due to polyethylene crystals as it was previously reported in literature. The X-ray pattern of EVA-2SNC and EVA-5SNC show the typical peak of EVA at 2θ = 21.5° and the broad peak of SNCs at 2θ = 30.3°. However, the other typical diffraction peaks of SNCs were shielded by the diffuse diffraction of EVA matrix.

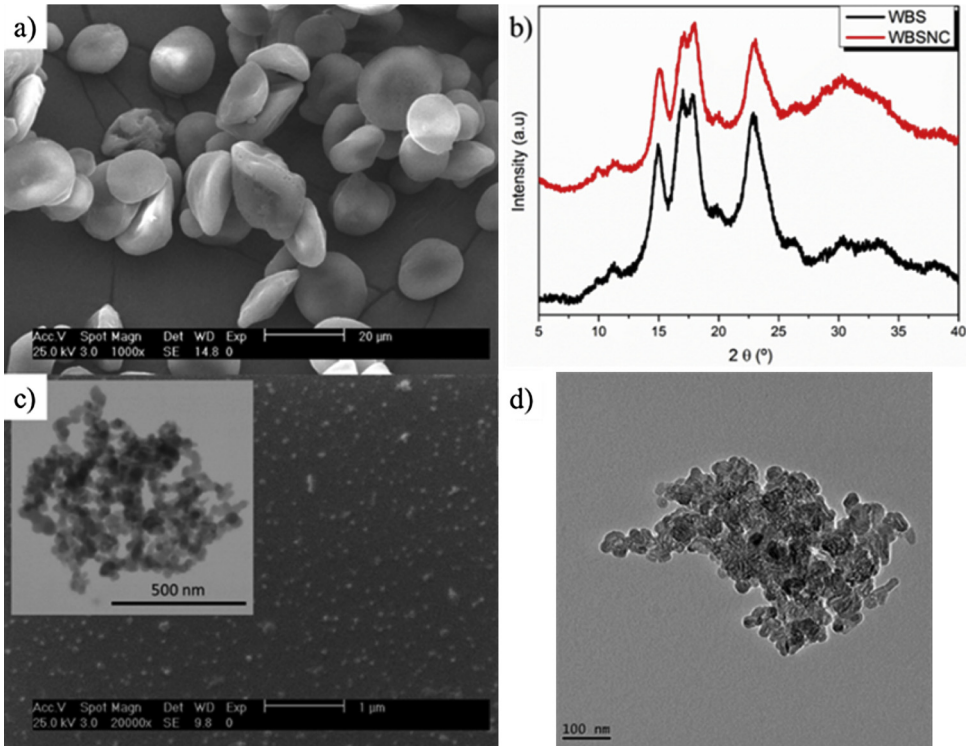

Fig. 1. Morphology and crystalline structure of WBS and SNCs. a) SEM micrograph of native WBS granules, b) X-ray patterns of WBS and WBSNC, c) SEM and FE-SEM (inset) micrographs of WBSNC and d) TEM micrograph of WBSNC.

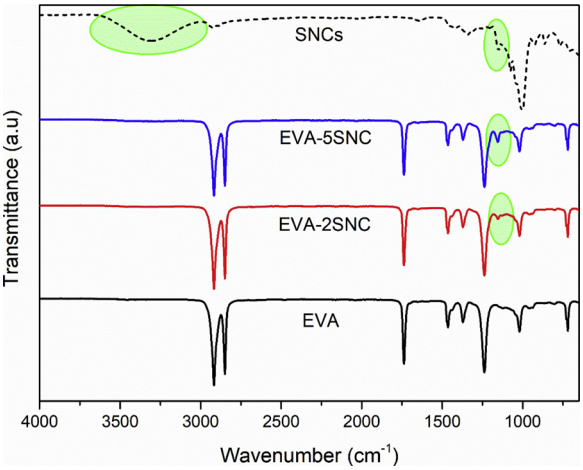

Fig. 2. Full ATR-FTIR spectra of SNCs, neat EVA and EVA/SNCs nanocomposites.

TM-AFM images, Figs. 5 and 6, have been also performed in order to study both the morphology and the dispersion of SNCs after their processing. In particular, in Fig. 5, 10 × 10μm TM-AFM height and phase images are reported for EVA-2SNC, while in Fig. 6, 3 × 3μm TM-AFM height and phase images are reported for EVA-5SNC. The inset of both figures represent the sections of SNCs.

In Fig. 5, thanks to the 10 × 10μm images, it is easy to note the good dispersion of the SNC in the EVA matrix, where no agglomeration are reported, in good agreement with previous results obtained from the previous FE-SEM analysis. Moreover, as indicated in the inset of the figure, the sections of the SNCs are reported in order to study their dimension after the processing. It is worth to note that no change on the dimension of the SNCs are reported, being their dimension comparable with the neat ones.

At difference of EVA-2SNC, nanocomposite obtained with 5 wt.% of SNCs presented small agglomerations, as indicated in Fig. 6. Even in this case, it is easy to note that the dimension and the morphology of the SNCs are not changed after the processing conditions when the nanocomposites are obtained. However, as expected, the small agglomerations found in the EVA-5SNCs can affect the mechanical performance of the nanocomposites.

The strong hydrogen bonding between the SNCs and the acetate groups of EVA lead to the improvement of the mechanical and thermal properties of the neat matrix. Tensile test of neat EVA and its nanocomposites were performed. The stress-strain curves are reported in Fig. 7.a.

Neat EVA shows the typical stress-strain curve of rubber polymers, characterized by high elongation at break and low elastic modulus. Strain hardening it was observed in all the samples due to the chain orientation in the stretching direction, leading to high stress at break (Ray, Khastgir, & Mukunda, 1993). The mechanical properties of neat EVA and EVA/SNCs nanocomposites are listed in Table 1.

The mechanical properties were significantly affected by the addition of SNCs. With increasing the amount of SNCs in the nanocomposites, the elastic modulus increased as compared with that of neat EVA. In particular, when 5 wt.% of SNCs has been added to EVA, a double elastic modulus has been obtained. However, the maximum stress was quite constant and the elongation at break decreased with the addition of SNCs, probably due to the small agglomerations obtained when 5 wt.% SNCs are added to EVA matrix. However, comparing our results with those of Pereda et al. (Pereda et al., 2014) for LDPE-based nanocomposites reinforced with unmodified starch nanocrystals processed by melt-processing, it is possible to notice that in our case the mechanical properties were still improved at 5 wt.% of nanocrystals.

In Fig. 7, the trend of mechanical properties as a function of SNCs content is shown. The modulus of the different samples was calculated at 300% of strain as well in order to study the effect of SNCs addition on the mechanical properties before the strain hardening of the matrix (Table 1). It is worth to note that the moduli at 300% of strain become higher with SNCs content in the EVA matrix, showing increases of

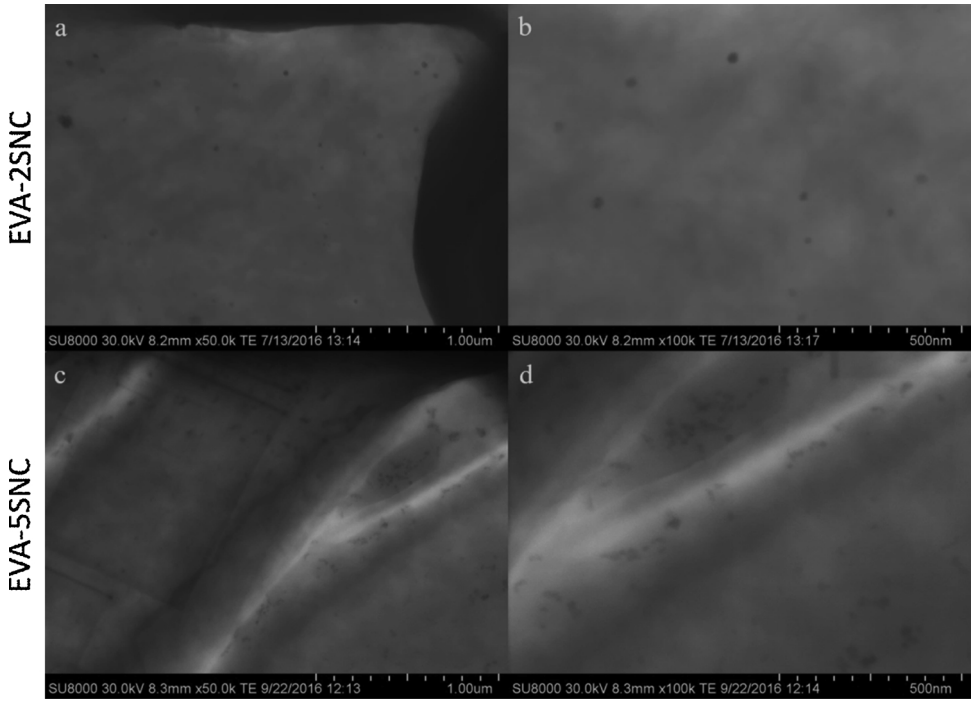

Fig. 3. FE-SEM images at different magnification of a) EVA-2SNC at 50,000x, b) EVA-2SNC at 100,000x, c) EVA-5SNC at 50,000x and d) EVA-5SNC at 100,000x.

around 100% and 140% for EVA-2SNC and EVA-5SNC, respectively. Moreover, the same trend was observed for the stress at 300% of strain, differently from the values of the maximum stress recorded. In fact, it was found that in EVA-2SNC and EVA-5SNC the stress at 300% show increases of 25% and 58%, respectively. However, a small variation has been observed at higher strain level (> 300% strain) where the modulus of pure EVA becomes slightly higher than those of its nanocomposites. It was observed that the nanocomposites undergo strain hardening at lower elongation percentages compared with neat EVA. This phenomenon might be attributed to the orientation of the crystalline polyethylene segments present in EVA, as reported in literature (Ray et al., 1993; Varghese, Bhagawan, Rao, & Thomas, 1995). In case of EVA-2SNC and EVA-5SNC as the amount of SNCs increased, the degree of crystallinity increased and the mobility of the polymer chains was restricted, leading to lower values of elongation at break and maximum stress as compared with neat EVA. Thus, the decrease of the strain at break of the EVA/SNC nanocomposites was directly related with crystallinity increase as shown in Table 2, where the DSC results are reported.

A T_g at around -26 °C was observed for neat EVA and it was related to the amorphous phase, consisting of amorphous PE and amorphous VA segments as previously reported in literature (Nöchel et al., 2014; Reding, Faucher, & Whitman, 1962). No changes were observed in the T_g values for the nanocomposites with respect to neat EVA. The results in terms of T_g, T_m, T_c, ΔH_m, ΔH_c and X_c are summarized on Table 2.

Neat EVA had a T_m of 86 °C and a T_c of about 70 °C. No variations in melting and crystallization temperatures were observed by DSC analyses, while an increase of enthalpy of fusion upon incorporation of SNCs is reported in Table 2. These results suggest that the increase of SNCs content improved the degree of crystallinity of EVA matrix likely due to the nucleation effect of the SNCs. Similar results were showed by Zou et al. (Zou et al., 2011), obtaining higher values of ΔH_m for waterborne polyurethanes/SNCs nanocomposites compared with that of the neat polymer thanks to the nucleation effect of SNCs. The same phenomenon was reported by Viguié et al. (Viguié, Molina-Boisseau, & Dufresne, 2007) for thermoplastic starch nanocomposites reinforced with SNCs.

The dynamic mechanical properties of neat EVA and its EVA/SNCs nanocomposites were studied by DMA technique. The storage modulus (E'), the loss modulus (E") and dumping factor (tan δ) as a function of temperature are shown in Fig. 8. The peak temperatures in Fig. 8.b and c are referred to the alpha-transition (glass transition) of EVA.

At low temperature, below T_g, the storage modulus underwent a slight enhancement with respect to the neat matrix upon addition of the

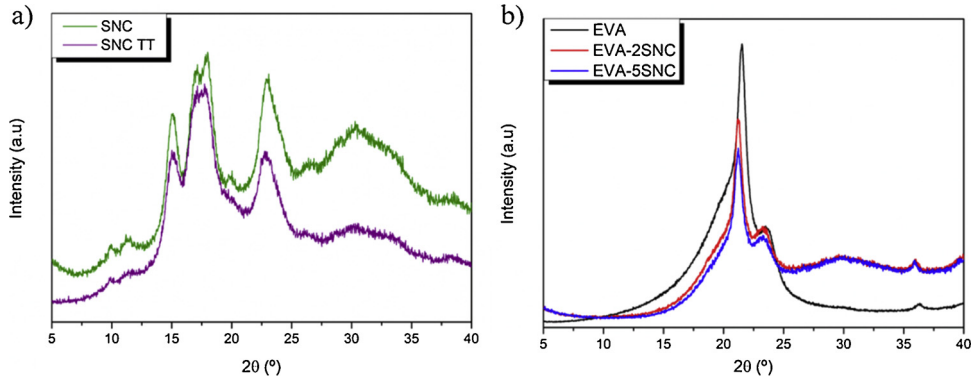

Fig. 4. XRD patterns of a) neat and annealed SNCs and b) neat EVA and its nanocomposites.

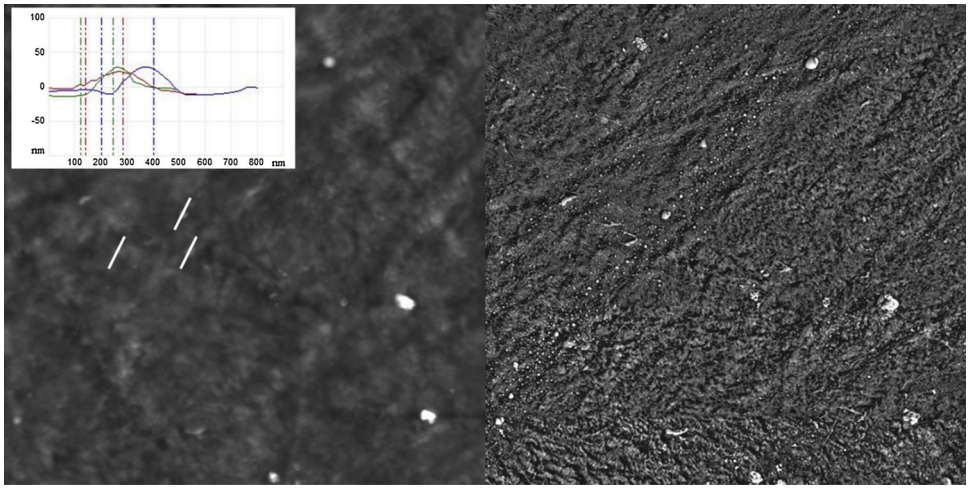

Fig. 5. 10 × 10μm TM-AFM height and phase images for EVA-2SNC.

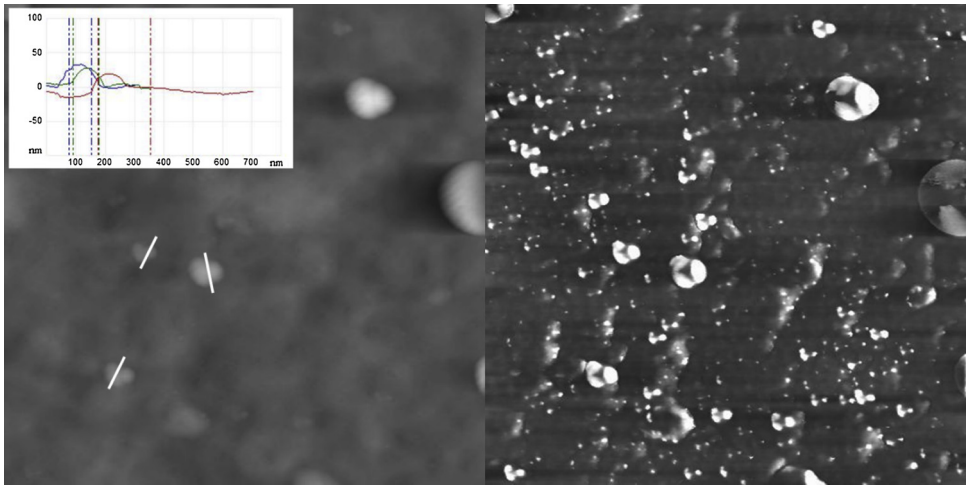

Fig. 6. 3 × 3μm TM-AFM height and phase images for EVA-5SNC.

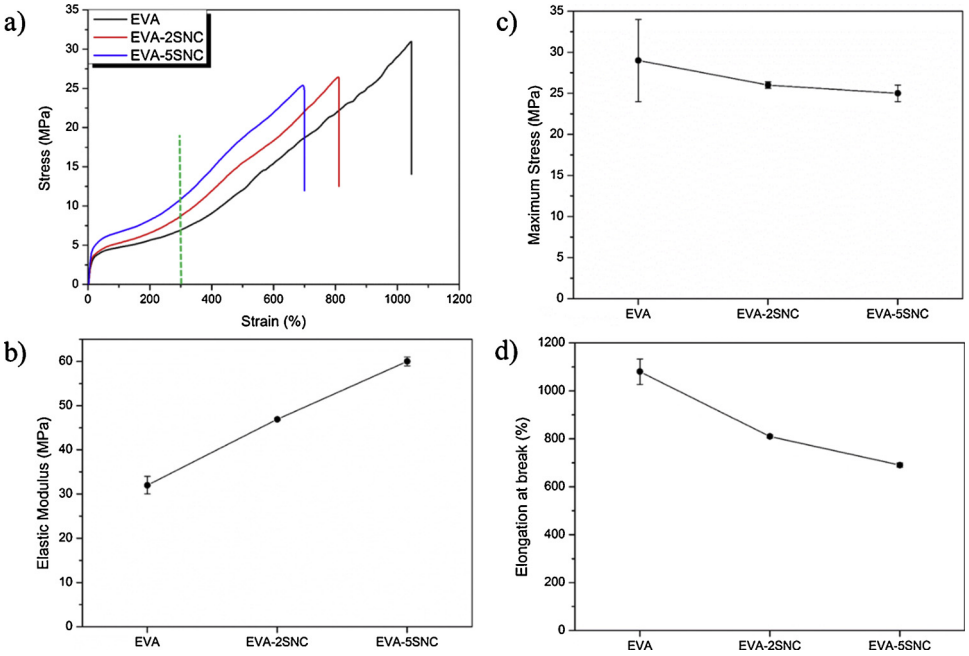

Fig. 7. a) Stress-strain curves of neat EVA and its nanocomposite. Trend of mechanical properties as a function of SNCs content. b) Elastic Modulus, c) Maximum Stress and d) Elongation at break.

Table 1
Mechanical properties of neat EVA and its nanocomposites.

Sample	Elastic Modulus (MPa)	Maximum Stress (MPa)	Elongation at break (%)	Stress at 300 % (MPa)	Modulus at 300 % (MPa)
EVA	32 ± 2	29 ± 5	1080 ± 53	6.96 ± 0.53	1.45 ± 0.48
EVA-2SNC	47 ± 1	26 ± 1	810 ± 7	8.73 ± 0.05	2.96 ± 0.09
EVA-5SNC	60 ± 1	25 ± 1	690 ± 9	10.96 ± 0.14	3.53 ± 0.08

Table 2
Thermal properties and degree of crystallinity.

Samples	T_c (°C)	T_m (°C)	ΔH_m (J/g)	X_c (%)	T_g (°C)
EVA	70	86	53	18	−26
EVA-2SNC	71	87	69	24	−26
EVA-5SNC	71	87	73	25	−26

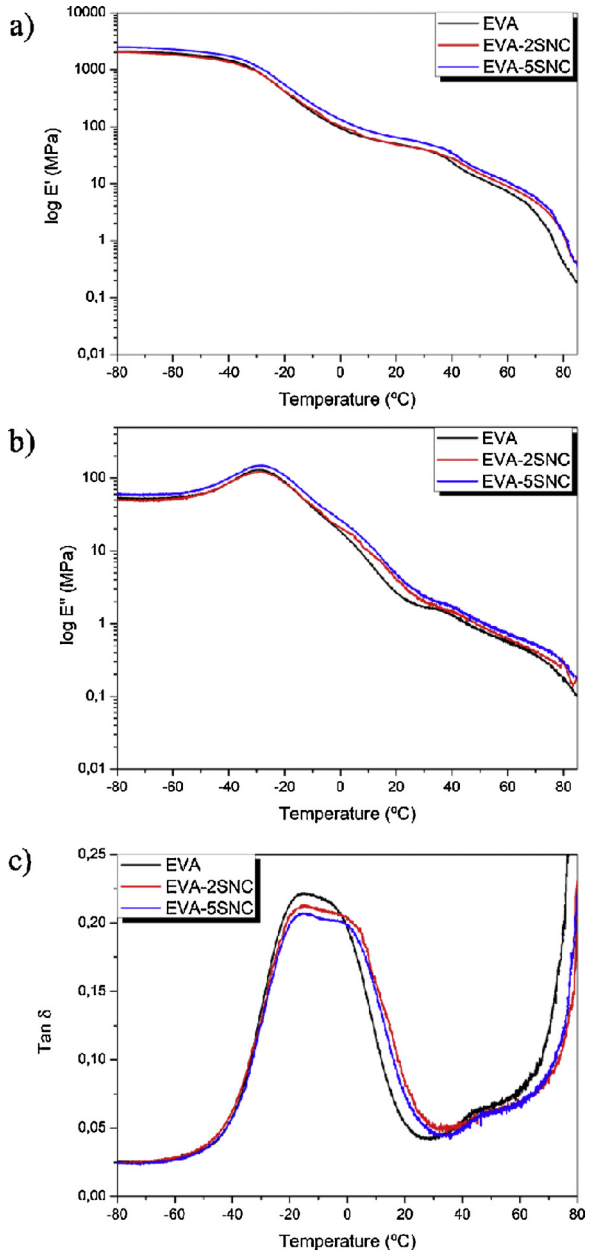

Fig. 8. Dynamic mechanical properties: a) storage modulus (E'), b) loss modulus (E") and c) damping factor (tanδ) of neat EVA and EVA/SNCs nanocomposites as a function of temperature.

nanoparticles. This behavior was expected as reported in literature for elastomeric matrices reinforced with SNCs (Haaj et al., 2014; Y. Wang et al., 2010) and it is attributed to the relative low difference between the modulus of the glassy matrix and that of the nanofiller network, considering the low filler amount. Thus, neat EVA in the glass state showed relatively high E' values (~ 2000 MPa) that increased by 500 MPa after addition of 5 wt.% of SNCs. No significant changes were observed after the addition of 2 wt.% of SNCs. Similar results were observed in waterborne polyurethane/SNCs systems as well (Zou et al., 2011). The slight enhancement of the storage modulus, as the result of the filler addition, was observed also in the rubbery region, indicating the presence of EVA-SNCs interfacial interactions. This leads to a slight delay on the drop of the E' curve corresponding to the melting of PE crystals. Moreover, the peak width of tanδ increased adding SNCs, indicating higher internal friction caused by EVA-SNCs interaction. Similar results were reported for EVA/CNC nanocomposites, where the interfacial interaction between CNCs and EVA matrix was confirmed by the increase of the intensity and peak width corresponding to the T_g of EVA (Ma, Jiang, Hoch, Dong, & Chen, 2015).

Finally, the thermal stability of the EVA/SNCs nanocomposites was studied by thermogravimetric analysis conducted under dynamic mode. Fig. 9 shows the TGA and its derivate (DTG) curves of the nanocomposite films as well as of neat EVA under nitrogen atmosphere. Thermal degradation of EVA takes place in two steps as it was previously reported in literature (Zanetti et al., 2001). In the first stage, deacylation with the elimination of acetic acid and the formation of double bonds occurs in the range of 270–380 °C. At temperatures higher than 380 °C, thermal degradation of the ethylene-co-acetylene random copolymer resulting from deacylation takes place.

The weight loss curves of the nanocomposites (Fig. 9) display a slight stabilization of about 10 °C, thus SNCs did not change the nature of degradation, but alters the temperature for maximum degradation. EVA-2SNC showed the initial degradation temperature ($T_{5\%}$) at 340 °C, EVA-5SNC showed it at 326 °C while neat EVA showed its $T_{5\%}$ at about 328 °C. The first maximum degradation temperature (T_{maxI}) was about 353 °C for both EVA-2SNC and EVA-5SNC whereas T_{maxI} for neat EVA was about 342 °C. Finally, the second maximum degradation temperature (T_{maxII}) was about 467 °C for both the EVA-SNCs nanocomposites,

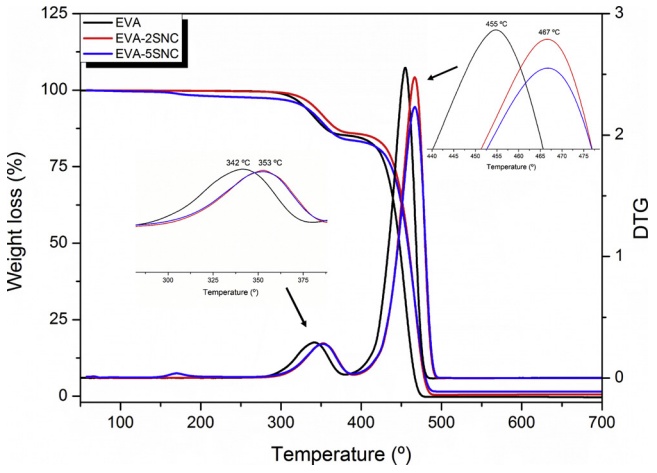

Fig. 9. TGA and DTG curves of neat EVA and its nanocomposites.

while neat EVA had its T_{maxII} at about 455 °C as it is showed in Fig. 9. Furthermore, a reduction of almost 2 wt.% was observed at 170 °C, corresponding to the degradation temperature of SNCs. The improvement in thermal stability was attributed to the homogeneous dispersion of SNCs, originated from the interaction between the hydroxyl groups on the SNCs surface and acetate groups of EVA. The increase on the thermal stability thanks to the interaction between EVA and nanofillers was already reported in literature, *i.e.* for EVA/Halloysite nanotubes nanocomposites (Bidsorkhi et al., 2015) and EVA/sepiolite nanocomposites (Bidsorkhi et al., 2014). Furthermore, the thermal stabilizing effect of SNCs due to the strong interaction between the OH-group on the SNCs surface and the polymer matrix was already reported for, *i.e.*, waterborne polyurethane/SNCs nanocomposites (Y. Wang et al., 2010) and in starch/SNCs nanocomposites (Li et al., 2015).

4. Conclusions

Green nanocomposites based on EVA and SNCs were successfully prepared by extrusion without lose their crystalline nature. DSC analysis showed the increase of the degree of crystallinity when higher amount of SNCs were loaded into the EVA matrix. The different changes in the FTIR spectra of EVA/SNCs nanocomposites compared to that of neat EVA were attributed to the positive interactions between the vinyl acetate groups of the matrix and the hydroxyl groups of SNCs. These physical interactions were reflected in the good and homogeneous dispersion of the nanofillers into the polymer matrix and on the enhanced mechanical properties of the nanocomposites. Indeed, adding 2 wt.% and 5 wt.% of SNCs into the EVA matrix, the elastic modulus increases around 50% and 100% respectively, comparing with the neat matrix, without variation on the maximum stress. Moreover, thermal stability of the prepared nanocomposites was improved of about 10 °C by the incorporation of up to 2 wt.% of SNCs. This work provided important information about the possibility to introduce SNCs in a polymeric matrix by melt-processing and about their use to improve EVA performances thanks to hydrogen bonding interaction between the matrix and the nanofillers.

Acknowledgements

Authors thank the Spanish Ministry of Economy, Industry and Competitiveness (MINEICO) for MAT2017-88123-P and M-ERANET POLYMAGIC: PCIN-2017-036. L.P. acknowledges the “Ramon y Cajal” (RYC-2014-15595) contract from the MINEICO. JMR is a FRS-FNRS research associate. The authors also thank CSIC for the I-Link project (I-Link1149).

References

Alakrach, A., Osman, A. F., Noriman, N., Betar, B., & Dahham, O. S. (2016). Thermal properties of ethyl vinyl acetate (EVA)/montmorillonite (MMT) nanocomposites for biomedical applications. *MATEC Web of Conferences, 78*, 01074.

Bidsorkhi, H. C., Adelnia, H., Pour, R. H., & Soheilmoghaddam, M. (2015). Preparation and characterization of ethylene-vinyl acetate/halloysite nanotube nanocomposites. *Journal of Materials Science, 50*(8), 3237–3245.

Bidsorkhi, H. C., Soheilmoghaddam, M., Pour, R. H., Adelnia, H., & Mohamad, Z. (2014). Mechanical, thermal and flammability properties of ethylene-vinyl acetate (EVA)/sepiolite nanocomposites. *Polymer Testing, 37*, 117–122.

Brogly, M., Nardin, M., & Schultz, J. (1997). Effect of vinylacetate content on crystallinity and second-order transitions in ethylene—vinylacetate copolymers. *Journal of Applied Polymer Science, 64*(10), 1903–1912.

Carvalho, A. J. F. (2013). 7 - Starch: Major sources, properties and applications as thermoplastic materials. In S. Ebnesajjad (Ed.). *Handbook of biopolymers and biodegradable plastics* (pp. 129–152). Boston: William Andrew Publishing.

Chauve, G., Heux, L., Arouini, R., & Mazeau, K. (2005). Cellulose poly (ethylene-co-vinyl acetate) nanocomposites studied by molecular modeling and mechanical spectroscopy. *Biomacromolecules, 6*(4), 2025–2031.

Chen, Y., Cao, X., Chang, P. R., & Huneault, M. A. (2008). Comparative study on the films of poly (vinyl alcohol)/pea starch nanocrystals and poly (vinyl alcohol)/native pea starch. *Carbohydrate Polymers, 73*(1), 8–17.

Darder, M., Aranda, P., & Ruiz-Hitzky, E. (2007). Bionanocomposites: A new concept of ecological, bioinspired, and functional hybrid materials. *Advanced Materials, 19*(10), 1309–1319.

Fredriksson, H., Silverio, J., Andersson, R., Eliasson, A. C., & Åman, P. (1998). The influence of amylose and amylopectin characteristics on gelatinization and retrogradation properties of different starches. *Carbohydrate Polymers, 35*(3), 119–134.

Gao, F., Beyer, G., & Yuan, Q. (2005). A mechanistic study of fire retardancy of carbon nanotube/ethylene vinyl acetate copolymers and their clay composites. *Polymer Degradation and Stability, 89*(3), 559–564.

Goffin, A.-L., Habibi, Y., Raquez, J.-M., & Dubois, P. (2012). Polyester-grafted cellulose nanowhiskers: A new approach for tuning the microstructure of immiscible polyester blends. *ACS Applied Materials & Interfaces, 4*(7), 3364–3371.

Gong, B., Liu, W., Tan, H., Yu, D., Song, Z., & Lucia, L. A. (2016). Understanding shape and morphology of unusual tubular starch nanocrystals. *Carbohydrate Polymers, 151*, 666–675.

Haaj, S. B., Thielemans, W., Magnin, A., & Boufi, S. (2014). Starch nanocrystal stabilized pickering emulsion polymerization for nanocomposites with improved performance. *ACS Applied Materials & Interfaces, 6*(11), 8263–8273.

Hebeish, A., El-Rafie, M., El-Sheikh, M., & El-Naggar, M. E. (2014). Ultra-fine characteristics of starch nanoparticles prepared using native starch with and without surfactant. *Journal of Inorganic and Organometallic Polymers and Materials, 24*(3), 515–524.

Jiahui, Y., Fujin, A., Alain, D., Shanjun, G., Jin, H., & R. C. P (2008). Structure and Mechanical Properties of Poly(lactic acid) Filled with (Starch nanocrystal)-graft-poly (ε-caprolactone). *Macromolecular Materials and Engineering, 293*(9), 763–770.

Khodkar, F., & Ebrahimi, N. G. (2011). Effect of irradiation on mechanical and structural properties of ethylene vinyl acetate copolymers hollow fibers. *Journal of Applied Polymer Science, 119*(4), 2085–2092.

Kizil, R., Irudayaraj, J., & Seetharaman, K. (2002). Characterization of irradiated starches by using FT-Raman and FTIR spectroscopy. *Journal of Agricultural and Food Chemistry, 50*(14), 3912–3918.

Labet, M., Thielemans, W., & Dufresne, A. (2007). Polymer grafting onto starch nanocrystals. *Biomacromolecules, 8*(9), 2916–2927.

Le Corre, D., Bras, J., & Dufresne, A. (2010). Starch nanoparticles: A review. *Biomacromolecules, 11*(5), 1139–1153.

LeCorre, D., Bras, J., & Dufresne, A. (2011). Influence of botanic origin and amylose content on the morphology of starch nanocrystals. *Journal of Nanoparticle Research, 13*(12), 7193–7208.

LeCorre, D., Bras, J., & Dufresne, A. (2012). Influence of native starch's properties on starch nanocrystals thermal properties. *Carbohydrate Polymers, 87*(1), 658–666.

Li, X., Qiu, C., Ji, N., Sun, C., Xiong, L., & Sun, Q. (2015). Mechanical, barrier and morphological properties of starch nanocrystals-reinforced pea starch films. *Carbohydrate Polymers, 121*, 155–162.

Lin, N., Huang, J., Chang, P. R., Anderson, D. P., & Yu, J. (2011). Preparation, modification, and application of starch nanocrystals in nanomaterials: A review. *Journal of Nanomaterials, 2011*, 20.

Lopez-Rubio, A., Flanagan, B. M., Gilbert, E. P., & Gidley, M. J. (2008). A novel approach for calculating starch crystallinity and its correlation with double helix content: A combined XRD and NMR study. *Biopolymers: Original Research on Biomolecules, 89*(9), 761–768.

Ma, P., Jiang, L., Hoch, M., Dong, W., & Chen, M. (2015). Reinforcement of transparent ethylene-co-vinyl acetate rubber by nanocrystalline cellulose. *European Polymer Journal, 66*, 47–56.

Morlat-Therias, S., Fanton, E., Gardette, J.-L., Peeterbroeck, S., Alexandre, M., & Dubois, P. (2007). Polymer/carbon nanotube nanocomposites: Influence of carbon nanotubes on EVA photodegradation. *Polymer Degradation and Stability, 92*(10), 1873–1882.

Mutungi, C., Passauer, L., Onyango, C., Jaros, D., & Rohm, H. (2012). Debranched cassava starch crystallinity determination by Raman spectroscopy: Correlation of features in Raman spectra with X-ray diffraction and 13C CP/MAS NMR spectroscopy. *Carbohydrate Polymers, 87*(1), 598–606.

Navarro-Baena, I., Kenny, J. M., & Peponi, L. (2014). Thermally-activated shape memory behaviour of bionanocomposites reinforced with cellulose nanocrystals. *Cellulose, 21*(6), 4231–4246.

Nöchel, U., Kumar, U. N., Wang, K., Kratz, K., Behl, M., & Lendlein, A. (2014). Triple-Shape Effect with Adjustable Switching Temperatures in Crosslinked Poly [ethylene-co-(vinyl acetate)]. *Macromolecular Chemistry and Physics, 215*(24), 2446–2456.

Peeterbroeck, S., Alexandre, M., Jérôme, R., & Dubois, P. (2005). Poly(ethylene-co-vinyl acetate)/clay nanocomposites: Effect of clay nature and organic modifiers on morphology, mechanical and thermal properties. *Polymer Degradation and Stability, 90*(2), 288–294.

Peponi, L., Puglia, D., Torre, L., Valentini, L., & Kenny, J. M. (2014). Processing of nanostructured polymers and advanced polymeric based nanocomposites. *Materials Science and Engineering R Reports, 85*(1), 1–46.

Pereda, M., Kissi, N. E., & Dufresne, A. (2014). Extrusion of polysaccharide nanocrystal reinforced polymer nanocomposites through compatibilization with poly (ethylene oxide). *ACS Applied Materials & Interfaces, 6*(12), 9365–9375.

Rajisha, K., Maria, H., Pothan, L., Ahmad, Z., & Thomas, S. (2014). Preparation and characterization of potato starch nanocrystal reinforced natural rubber nanocomposites. *International Journal of Biological Macromolecules, 67*, 147–153.

Ray, I., Khastgir, D., & Mukunda, P. (1993). Effect of strain rate and temperature on stress-strain properties of EVA-LDPE blends and the mechanism of strain hardening. *Die Angewandte Makromolekulare Chemie: Applied Macromolecular Chemistry and Physics, 205*(1), 59–74.

Reding, F., Faucher, J., & Whitman, R. (1962). Glass transitions in ethylene copolymers and vinyl homopolymers and copolymers. *Journal of Polymer Science, 57*(165), 483–498.

Sengupta, R., Bhattacharya, M., Bandyopadhyay, S., & Bhowmick, A. K. (2011). A review

on the mechanical and electrical properties of graphite and modified graphite reinforced polymer composites. *Progress in Polymer Science, 36*(5), 638–670.
Sessini, V., Arrieta, M. P., Kenny, J. M., & Peponi, L. (2016). Processing of edible films based on nanoreinforced gelatinized starch. *Polymer Degradation and Stability, 132*, 157–168.
Sessini, V., Arrieta, M. P., Fernández-Torres, A., & Peponi, L. (2018). Humidity-activated shape memory effect on plasticized starch-based biomaterials. *Carbohydrate Polymers, 179*, 93–99.
Sessini, V., Navarro-Baena, I., Arrieta, M. P., Dominici, F., López, D., Torre, L., ... Peponi, L. (2018). Effect of the addition of polyester-grafted-cellulose nanocrystals on the shape memory properties of biodegradable PLA/PCL nanocomposites. *Polymer Degradation and Stability, 152*, 126–138.
Sonia, A., & Dasan, K. P. (2013). Celluloses microfibers (CMF)/poly (ethylene-co-vinyl acetate)(EVA) composites for food packaging applications: A study based on barrier and biodegradation behavior. *Journal of Food Engineering, 118*(1), 78–89.
Varghese, H., Bhagawan, S., Rao, S. S., & Thomas, S. (1995). Morphology, mechanical and viscoelastic behaviour of blends of nitrile rubber and ethylene-vinyl acetate copolymer. *European Polymer Journal, 31*(10), 957–967.
Viguié, J., Molina-Boisseau, S., & Dufresne, A. (2007). Processing and characterization of waxy maize starch films plasticized by sorbitol and reinforced with starch nanocrystals. *Macromolecular Bioscience, 7*(11), 1206–1216.
Wang, T. L., Bogracheva, T. Y., & Hedley, C. L. (1998). Starch: As simple as A, B, C? *Journal of Experimental Botany, 49*(320), 481–502.
Wang, Y., Tian, H., & Zhang, L. (2010). Role of starch nanocrystals and cellulose whiskers in synergistic reinforcement of waterborne polyurethane. *Carbohydrate Polymers, 80*(3), 665–671.
Yixiang, X., N, S. E., Cory, G., Melissa, T., Dmitry, P., Zachary, H., et al. (2014). Morphological, structural, and thermal properties of starch nanocrystals affected by different botanic origins. *Cereal Chemistry, 91*(4), 383–388.
Zanetti, M., Camino, G., Thomann, R., & Mülhaupt, R. (2001). Synthesis and thermal behaviour of layered silicate–EVA nanocomposites. *Polymer, 42*(10), 4501–4507.
Zhang, F., & Sundararaj, U. (2004). Nanocomposites of ethylene-vinyl acetate copolymer (EVA) and organoclay prepared by twin-screw melt extrusion. *Polymer Composites, 25*(5), 535–542.
Zou, J., Zhang, F., Huang, J., Chang, P. R., Su, Z., & Yu, J. (2011). Effects of starch nanocrystals on structure and properties of waterborne polyurethane-based composites. *Carbohydrate Polymers, 85*(4), 824–831.